Journal of Thermal Science Vol.31, No.6 (2022) 1868−1880

https://doi.org/10.1007/s11630-021-1466-8 **Article ID: 1003-2169(2022)06-1868-13**

Analysis of the Light Concentration Loss of a Fresnel CPV/T System after Dust Accumulation

ZHAO Ning[1], YAN Suying[1*], MA Xiaodong[1], WU Ze[1], MING Tingzhen[2], ZHAO Xiaoyan[1], ZHANG Na[3]

1. College of Energy and Power Engineering, Inner Mongolia University of Technology, Hohhot 010051, China
2. School of Civil Engineering and Architecture, Wuhan University of Technology, Wuhan 430070, China
3. Institute of Engineering Thermophysics, Chinese Academy of Sciences, Beijing 100190, China

Abstract: Dust accumulation is one of the reasons for the performance degradation of concentrating photovoltaic and thermal (CPV/T) systems due to the deposition of dust particles with different compositions, shapes, sizes, and masses. In this work, an optical model was developed to investigate the influence of the particle size, diameter, shape, and deposition density on the light concentration efficiency, using the Monte Carlo raytracing (MCRT) method in the Tracepro software. The triangular particles had a larger influence on the light ray deflection and energy flux degradation than the circular and square particles. An average increase in the dust density of 1 g/m^2 decreased the light concentration efficiency of particles with sizes smaller than 50 μm and 60 μm by 3.31% and 3.26%, respectively. Furthermore, the effect of the incidence angle on the light concentration efficiency was considered at an angle less than 2°.

Keywords: dust accumulation, Fresnel CPV/T system, light concentration efficiency, Monte Carlo raytracing

1. Introduction

Photovoltaic (PV) and concentrating photovoltaic/thermal (CPV/T) systems are useful and feasible solutions for future energy generation [1, 2]. However, the progress of these technologies is subject to environmental influences and geographical conditions in large-scale applications [3]. Dust accumulation is the most important and common reason for a decreased output efficiency of CPV/T systems. The dust particles reduce the amount of solar radiation passing through the lens and decrease the transmittance, causing heterogeneous energy flow on the surface of the CPV/T receiver [4–6] and substantially reducing the thermal and electrical efficiency of the solar concentrating system [7–10].

The primary factors affecting the concentration efficiency are the type, density, shape, size, and other physical and chemical properties of the dust particles in the accumulated dust [11, 12]. Different types of samples, including ash, soil, sand, cement, charcoal, calcium, and other dust types, have been used to investigate the soiling effect on the optical performance [13–15]. Salari and Hakkaki-Fard [16] numerically investigated the dust effects and found that an increase in the dust density from 0 g/m^2 to 8 g/m^2 resulted in a reduction in the electrical efficiency of 26.36% and 26.42% in the PV and PV/T system, respectively. The reduction in the PV output of PV panels caused by increasing dust density

Special column: Built Thermal Environment GE: DAI Yanjun
Received: Aug 20, 2020 Corresponding author: YAN Suying E-mail: yansy@imut.edu.cn

Nomenclature

Acronyms

CFD	Computational fluid dynamics
CPV	Concentrating photovoltaic
CPV/T	Concentrating photovoltaic and thermal
CSP	Concentrating solar power
EDS	Energy Dispersive X-ray Spectroscopy
MCRT	Monte Carlo ray-tracing
MS	Markov regime-switching
PMMA	Polymethyl methacrylate
PV	Photovoltaic
PVC	Polyvinyl chloride
PV/T	Photovoltaic and thermal
RMSE	Root mean square error
SEM	Scanning Electron Microscopy
SOG	Silicon on glass
XRD	X-ray powder diffraction

Greek symbols

η_c	light concentration efficiency before dust accumulation/%
η_d	light concentration efficiency after dust accumulation/%
η_{loss}	the loss rate of the light concentration efficiency/%
η_r	dust coefficient/%
ρ_{ave}	average dust density/g·m^{-2}
ω	density of dust particles/g·m^{-3}

Roman symbols

E_{ave}	average irradiance/W·m^{-2}
E_{max}	maximum irradiance/W·m^{-2}
E_{min}	minimum irradiance/W·m^{-2}
m	the mass of the dust/g
n	total number of experiments
S	the area of the Fresnel lens/m^2
T_{avg}	mean transmittance value/%
T_e	experimental transmittance value/%
V	volume of the accumulated dust/m^3

was also analyzed using computational fluid dynamics (CFD) simulation [17]. Hachicha et al. [18] reported that the dust accumulation increased by 5.44 g/m^2 after five months in an experiment in the United Arab Emirates. Boyle et al. [19] observed that the light transmittance decreased by 4.1% for each 1 g/m^2 of accumulated dust. Pan et al. [20] investigated the PV efficiency of glass coated with hydrophobic silica sol material exposed for 60 min with a 30° tilt angle and found the reduction was about 25.4%. In addition, artificial dust included local surface soil, ash, sand and droppings was used to investigate the effect of controlled deposition dust messes on light concentration efficiency [21–23]. Several dust deposition approaches have been reported such as manually sieveing, injecting, and the use of fan or wind tunnel [24–26]. The manual and free-fall approach [26] was adopted in this study because of its simplicity and the similarity of the deposition behaviors of the particles to natural deposition.

Experiments were conducted in different geographical areas to investigate the dust properties and the degradation of the output efficiency caused by dust deposition [27–31]. The chemical and textural properties of the accumulated dust particles were analyzed using scanning electron microscopy (SEM) and energy-dispersive X-ray spectroscopy [25, 32]. The results revealed that the shapes of dust particles are highly irregular [33]. Ghazi et al. [34] investigated the dust particle size and diameter in different areas of the world. Morphological factors such as the shape, edge sharpness and the degree of surface roughness affected the scattering characteristics of the particles [35]. El-Shobokshy and Hussein [36] observed that smaller dust particles resulted in a greater reduction in PV efficiency than larger particles. Heimsath and Nitz [37] used a Markov regime-switching (MS) method to analyze the impact of small-angle scattering and incidence angles on the electrical output performance using artificial soiling and desert dust.

Recently, some studies were conducted on the Fresnel lens of CPV/T to determine the optimum thermal and electrical output performance [38–41]. Dust accumulation also has a significant influence on the Fresnel lens of CPV/T systems [42]. In this study, the effect of dust deposition the Fresnel lens of a three-stage CPV/T system on light concentration efficiency is analyzed using simulations and experiments.

This study also presents a novel method in Section 2 to model dust particles accumulated on the Fresnel lens and represent the basis for the optical performance analysis in Section 4. The experimental method and light concentration index are presented in Section 3. The simulation and experimental results are described in Section 4. Dust particles with different shapes and diameters are analyzed, and a dust density range of 0 g/m^2 to 15 g/m^2 is considered. The energy flux density at different angles of incidence is investigated. Section 5 summarizes the conclusions.

2. System and Optical Simulation

2.1 Fresnel lens concentrating system

A CPV/T system coupled with a Fresnel lens (Fig. 1) was used in this study. The theoretical geometric concentration ratio and optical concentration ratio were 1000x and 800x, respectively. The system consists of a Fresnel lens (first stage), a light funnel (second stage), and a prism (third stage), which are made of PMMA, aluminum, and silicon on glass (SOG), respectively. The solar rays are vertically focused on the surface of the light funnel through the Fresnel lens; most of the light irradiates the cell directly, and some of the light is reflected by the light funnel and then transmitted to the solar cell. The light is reflected by the secondary light prism and is uniformly transmitted to the surface of the gallium arsenide cells. The parameters of the concentrating system are listed in Table 1.

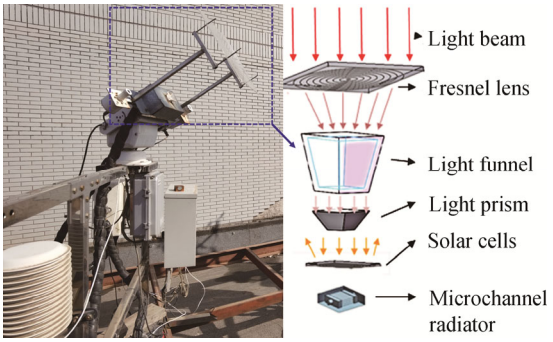

Fig. 1 Schematic diagram of the Fresnel lens concentrator system

Table 1 Parameters of the Fresnel lens system

Parameters	Value	Units
Length of the lens edge	330	mm
Focal length	350	mm
Ring spacing of the lens	1	mm
Thickness of the lens	5	mm
Reflective index	1.49	mm
Top part of light funnel	44×44	mm
Bottom of light funnel	19×19	mm
Height of the light funnel	30	mm
Homogenizer	19×19	mm
Bottom of optical prism	10×10	mm
Height of the optical prism	20	mm

2.2 Simulation model

The density of the dust particles ω is determined based on the mass of the dust particles m and the Fresnel lens area S as follows:

$$\omega = m/S \tag{1}$$

where m is the product of the average dust density ρ_{ave} and the volume of the accumulated dust V as:

$$m = \rho_{ave} V \tag{2}$$

We combine Eqs. (1) and (2) to obtain the dust density in Eq. (3):

$$\omega = \left(V \times \rho_{ave}\right)/S \tag{3}$$

A grid pattern was created on the surface of the Fresnel lens and the concept of the equivalent grain size [43] was used. The dust particles are assumed to be cylinders, triangles, and cuboids. The axial length of the geometrical bodies was 330 mm, the same as the side length of the Fresnel lens. The diameter of the cross-sectional areas was used instead of the diameter of the particles, and the particles of different diameters were used to compare the deposition densities for the same shape of dust particles. Cylinders, triangular prisms, and cuboids were simplified into circles, triangles, and squares according to the cross-sectional shape. The dust particle model was established in SolidWorks, as shown in Fig. 2. An orthogonal configuration of the linear array was performed to obtain grid models with different dust densities.

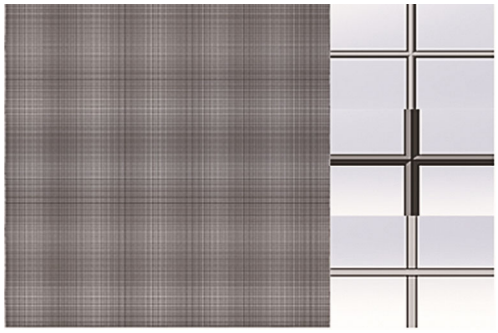

Fig. 2 Geometric array for determining the dust accumulation

The standard test condition (radiance: 1000 W/m^2; cell temperature: 25°C; sun spectrum: AM 1.5) was used in the simulation progress. The 500 nm wavelength was selected as the main wavelength because both the distribution of standard AM 1.5G spectrum curve and the spectral response curves of the three-junction solar cell. The external quantum efficiency of the solar cell and the AM 1.5G solar irradiance spectrum are shown in Fig. 3. The refraction coefficient, absorption coefficient, and transmission ratio of the dust model were 1.41, 0, and 1, respectively. The Monte Carlo ray-tracing (MCRT) method [44] was used to trace the optical rays on the Fresnel lens surface for different dust densities. Light travels in a straight line when it does not encounter obstacles; therefore, the smaller the measured angle, the greater the degree of light reflection is, i.e., the degree of change in the path of the light. The optical path before and after ray sorting in the three-stage Fresnel system is shown in Fig. 4.

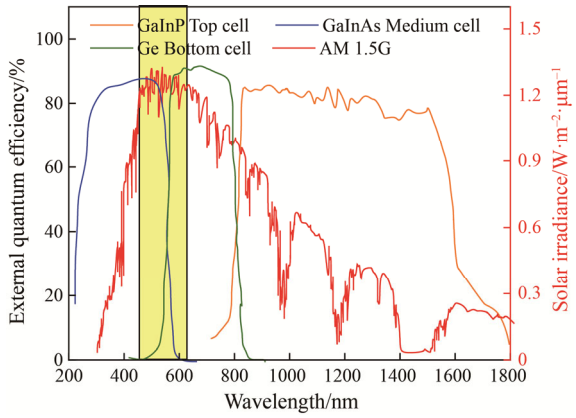

Fig. 3 The external quantum efficiency of the solar cell and the AM 1.5G spectrum

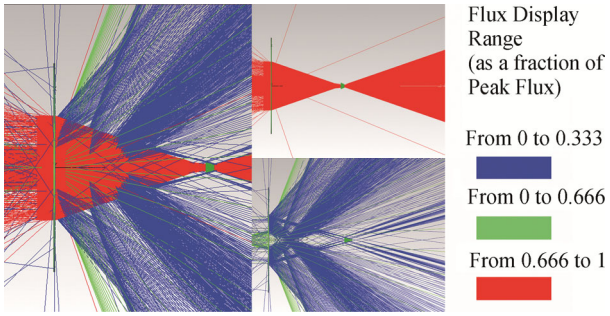

Fig. 4 Optical path before and after ray sorting

2.3 Model validation

Uncertainties in the MCRT method occur because of the random direction of the transmitted light when a single ray reaches a reflective surface [45]. The independence of the number of ray rings was verified to ensure the reliability of the simulation results. The cell surface energy and the light concentration efficiency of five schemes are compared, as shown in Table 2. Due to the accuracy of the computer configuration and the simulation results, the five schemes were averaged, and Scheme 3 was selected for the subsequent analyses. The deviations of each scheme are within 1%.

Table 2 Ray simulation results for determining the independence of the ring number

Scheme	Number of ray rings	Energy on the cell surface/W	Light concentration efficiency/%
1	100	85.721	78.867
2	200	85.997	78.969
3	300	85.849	78.882
4	400	85.883	78.864
5	500	85.812	78.799
Average		85.852	78.876

3. Experiment and Evaluation Index

3.1 Experimental method

The Fresnel lens was represented by several samples consisting of PMMA material with the same thickness; each lens sample had a dimension of 40 mm × 40 mm × 3 mm. Natural dust and artificial dust were investigated (Table 3) using X-Ray powder diffraction (XRD) measurements. The content and composition of the dust types were similar. The SiO_2 content of the artificial dust was higher than that of the natural dust. A sieve with a coarse aperture diameter was used to sift the artificial dust particles since the dust contained large particles. The dust with different masses was scattered on the sample surfaces using a free-fall approach, and a soft brush was used to distribute the particles uniformly. The dust was scattered and deposited on the samples until no particles slid off the surface when they were tilted at 90°. Measurements were used to ensure that all the particles adhered to the surface; the gravitational effect was ignored. The mass of the lens samples before and after dust deposition (shown in Fig. 5(a)) was measured using a BSA2245-CW balance (shown in Fig. 5(b)) with an accuracy of 0.0001 g. The difference between the initial mass (clean) and the mass of a sample with accumulated dust represented the mass of dust accumulated on the sample surface so that the dust accumulation density could be measured indirectly. The transmittance of the lens samples before and after the dust accumulation was measured using a Shimadzu UV-Vis3600 spectrophotometer (shown in Fig. 5(c)) with a precision of 1 nm. The clean sample was measured first to confirm the actual transmittance ranges of the PMMA lens samples after the spectrometer had been settled for about 20 min to promote stability. The transmittance of each lens was tested several times. The wavelength ranged from 200 nm to 1500 nm, corresponding to the spectral range of the three-junction solar cell. The root mean square errors (RMSE) of clean and dusty samples were measured; the mean value was obtained to minimize the measurement error. The RMSE is defined as:

$$\mathrm{RMSE}=\sqrt{\frac{1}{n}\sum_{i=1}^{n}\left(T_{\mathrm{e}}-T_{\mathrm{avg}}\right)^{2}} \tag{4}$$

where T_{e} and T_{avg} are the experimental value and mean of the transmittance, respectively, and n is the total number of experiments [46]. The closer the RMSE value to 0 is, the smaller the error is.

Table 3 Components of the natural dust and artificial dust

Dust type	Natural dust	Artificial dust
Components	Mass fraction	
SiO_2	53%	60%
$CaCO_3$	25%	20%
$NaAlSi_3O_6$	21%	18%

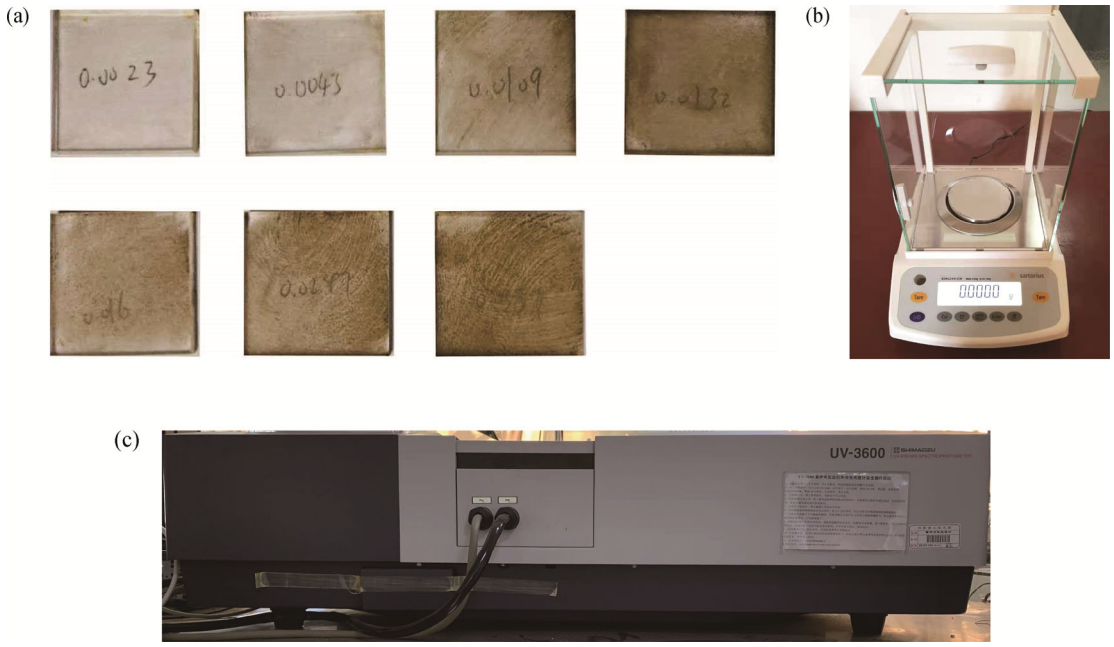

Fig. 5 Lens samples after dust deposition (a), the BSA2245-CW balance (b), and the UV-Vis3600 spectrophotometer (c)

3.2 Light concentration index

The dust coefficient η_r was used as an index to evaluate the effect of the dust accumulation on the light concentration efficiency. This approach minimized installation errors and the influence of solar radiation and temperature on the light concentration efficiency. This index is the ratio of the light concentration efficiency before and after the dust accumulation; the greater the value of the index, the cleaner the Fresnel lens surface is and the smaller the influence on the dust is. The dust coefficient η_r is calculated as follows:

$$\eta_r = \frac{\eta_d}{\eta_c} \tag{5}$$

where η_c and η_d are the light concentration efficiency before and after dust accumulation, respectively.

The dust on the surface of the Fresnel lens reduces the transmission of solar radiation, resulting in a decrease in solar radiation received by the cell surface. Since we wanted to conduct a quantitative analysis of the influence of different dust densities on the light concentration efficiency loss, the loss rate of the light concentration efficiency η_{loss} was used [47]. The greater the value of the loss rate, the greater the influence of the dust accumulation on the cell surface area is. The loss rate of the light concentration is calculated as follows:

$$\eta_{loss} = \frac{\eta_c - \eta_d}{\eta_c} \times 100\% \tag{6}$$

An uneven energy distribution refers to the energy density on the surface of the cell caused by the dispersion of sunlight passing through the Fresnel lens; this condition adversely affects the conversion efficiency of the solar cell. In the international standard IEC60904-9, the maximum and minimum values of the surface irradiance are used to represent the uneven energy distribution [48]:

$$N = \left(\frac{E_{max} - E_{min}}{E_{max} + E_{min}} \right) \cdot 100\% \tag{7}$$

where E_{max} and E_{min} are the maximum and the minimum irradiance values measured by the detectors, respectively. Therefore, the uniformity of the light spots is defined as ΔE=1–N. The system irradiance of the concentrator was simulated using Tracepro software. The minimum value was almost zero; therefore, the average irradiance E_{ave} was used instead of the minimum value, namely:

$$\Delta E = 1 - \frac{E_{max} - E_{ave}}{E_{max} + E_{ave}} \cdot 100\% \tag{8}$$

where the unit of irradiance is W/m^2.

4. Results and Discussion

4.1 Optical path changes

The average angle was selected after light filtering, and each light path angle of the dust model was measured. As shown in Fig. 6, for the same dust density and cross-sectional area, the three types of dust particles block out light in different sized areas on the lens surface, and the triangular shape has the minimum optical deflection angle. For the square and circular dust particles, some of the rays are refracted from the side of the dust particles and are refracted to the upper surface of the light prism through the Fresnel lens. The largest

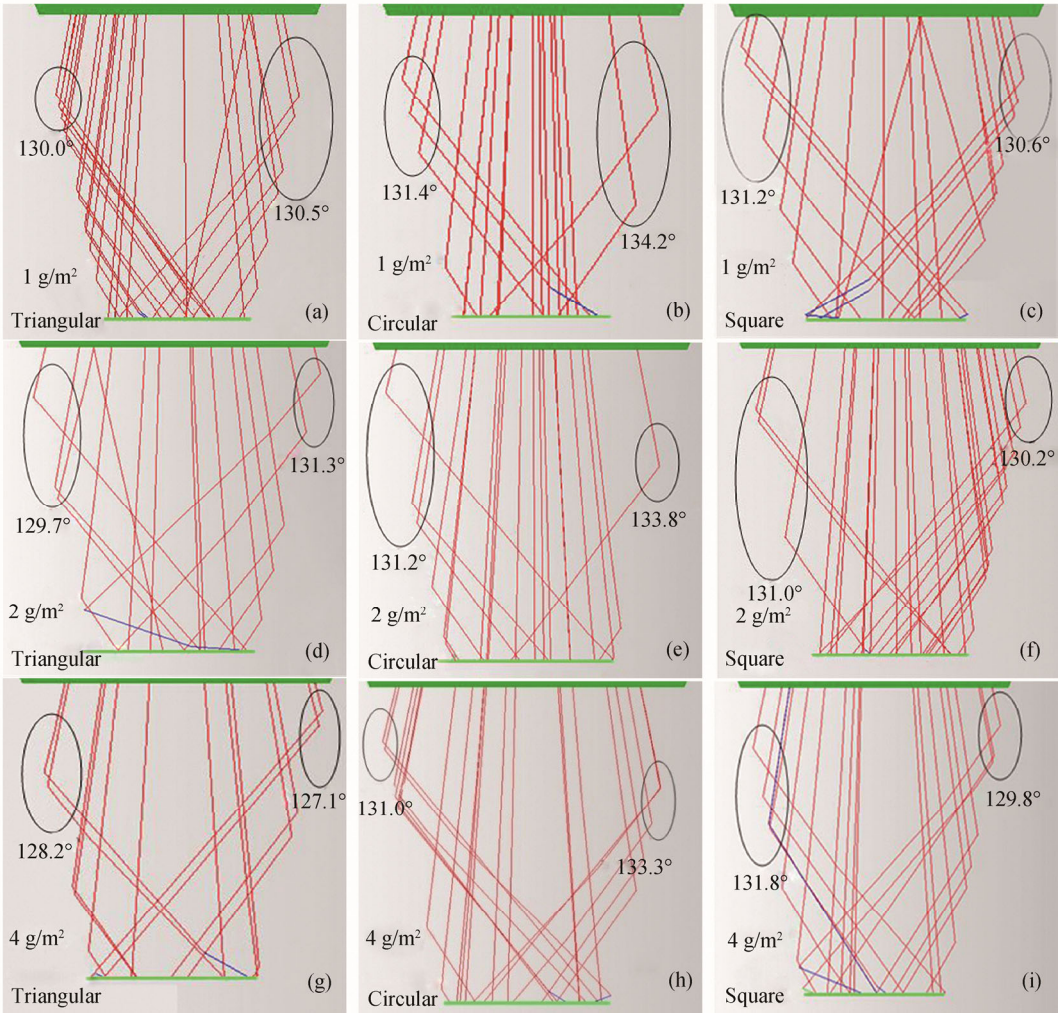

Fig. 6 Effects of the particle shape on the optical path angle

optical path changes and the greatest influence on the light concentration efficiency are observed for the triangular particles; in addition to the above reasons, energy loss occurs because of the phase distortion [49], which causes the light to be reflected and refracted many times.

Fig. 7 shows the effects of the particle diameter on the optical path angle for circular particles with a dust density of 1 g/m^2. Dust particles with a diameter of 10 μm result in the smallest optical path angle. In contrast, for the same deposition density, there are few dust particles with a large diameter, resulting in less light deflection. The reason is that there are more particles with a small diameter than larger diameter, thus minimizing the voids between the particles through which light can pass, except for the case when the dust density was sufficiently high to block all lights. The results indicate that dust particles with a smaller diameter have a greater influence on the optical light path.

4.2 Energy flux distribution

The energy flux distribution is shown in Fig. 8. An X-shape is visible on the clean (left) and dust-covered (right) surfaces because the solar radiation focused on the square optical prism after concentrated by the Fresnel lens. Subsequently, the solar rays spread outward from the cell surface, resulting in less energy flow at the center. The difference between the low-energy flow area and the edge is smaller in the dust-covered area, and the energy flux is lower after dust accumulation.

Fig. 9 shows the surface irradiance of the cell for the dust densities of 0.5 g/m^2, 1 g/m^2, 2 g/m^2, and 4 g/m^2. Multiple peaks and troughs can be observed in each case. The irradiance is radially symmetric around the center of the solar cell and decreases sharply at the edge. The reason is that the inherent structure of the Fresnel CPV/T system results in uneven energy distribution. The center shifts when the dust density is 4 g/m^2 because the larger the dust density, the smaller the mesh grid is, and the rays

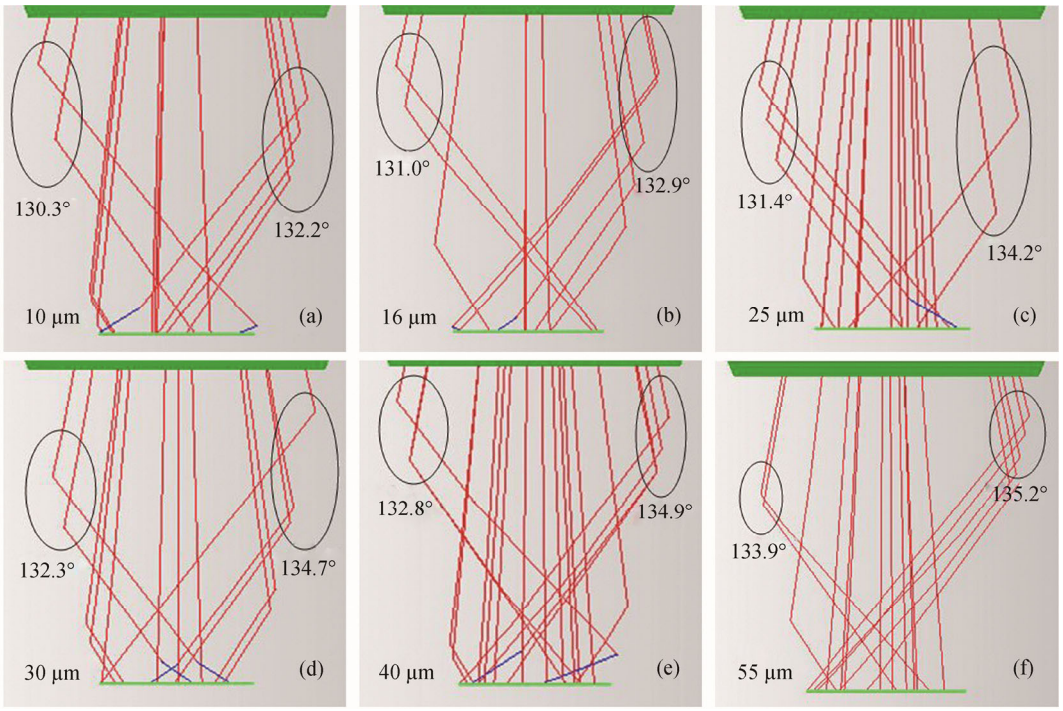

Fig. 7 Effects of the particle diameter on the optical path angle

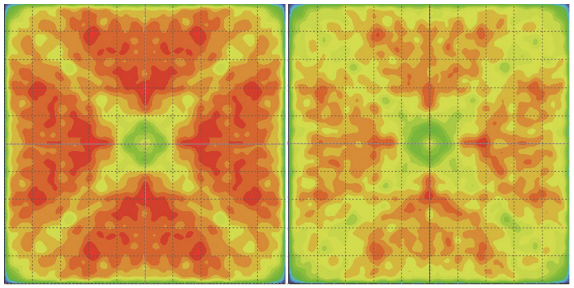

Fig. 8 Energy flux distribution before (left) and after (right) dust accumulation

cannot pass through the gaps between the dust, causing a change in the light path.

All dust particle shapes result in a significant change in energy density. The triangular dust particles have the largest influence on the energy density on the cell surface. The models of the triangular dust particles with dust densities of 0.5 g/m^2, 1 g/m^2, 2 g/m^2, and 4 g/m^2 exhibit decreases in the cell center irradiance of 13.25%, 14.46%, 30.12%, 16.88%, respectively. The irradiance for a density of 2 g/m^2 is greater than that for 4 g/m^2. The reason is that when the deposition density increases to a critical value, the dust particles have flattened the trough, and the irradiance at the X=0 position decreases at a slow rate. The models of the other dust particle shapes also result in different degrees of reduction in the irradiance for the four dust densities.

As shown in Fig. 10, as the dust density increases, the light concentration efficiency decreases. Compared to the clean state, the decrease in the light concentration efficiency for the circular, square, and triangular dust particles at 15 g/m^2 is 67.1%, 64.4%, and 69.5%, respectively. The dust particles with the equilateral triangle cross-section, which will significantly change the optical light path. The circular dust particles have a smooth surface that reflects much of the solar radiation, causing a loss in the light concentration efficiency. The square dust particles are perpendicular to the incident rays, and there is relatively little reflection loss. Therefore, the triangular dust particles have the greatest effect on the light concentration efficiency of the system. The optical spot uniformity also exhibits different trends for the different particle shapes. As the dust density increases, the light concentration efficiency and the spot uniformity decrease.

Fig. 11 shows the irradiance on the cell surface for dust particles of the same shape and different diameters. The irradiance of the solar cell shows a significant degradation (for each case) that depends on the dust density and the size of dust particles. The curves are quite similar for the different diameters, except for the curves with a diameter of 10 μm that exhibit less radial symmetry around the cell center. The reason is that for dust particles of the same shape and the same dust density, the smaller the dust particle size, the larger the dust deposition area is on the Fresnel lens surface. As a result, more optical rays are blocked by the finer dust, the light scattering is greater, and the energy density on the cell surface is lower.

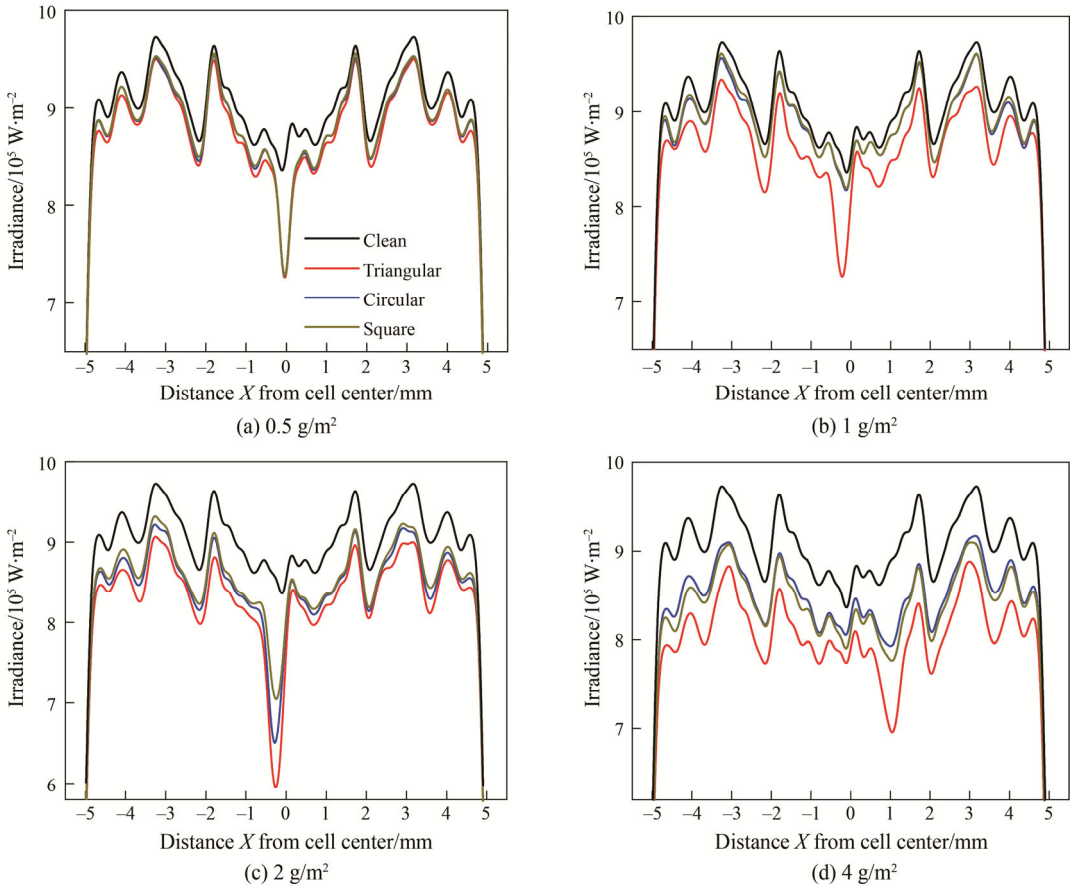

Fig. 9 Irradiance on the cell surface for different particle shapes

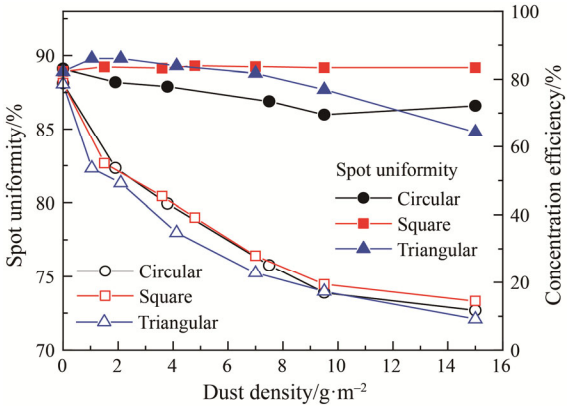

Fig. 10 Effect of the particle shape on the light concentration efficiency

Fig. 12 shows that the loss rate of the light concentration efficiency of the system increases with the increase in the dust density, whereas the dust coefficient decreases. As the dust density increases from 0 g/m^2 to 15 g/m^2, the dust coefficient decreases from 100% to 53.93%, 50.21%, 47.67% for the particle diameters of 50 μm, 30 μm, and 20 μm, respectively. The loss rate of the light concentration efficiency increases from 0% to 46.06%, 49.79%, and 52.33%, respectively. The loss rate shows an initial rapid increase trend, followed by a slower increase. At the same dust density, the larger the particle diameter is, the larger the dust coefficient is.

4.3 Energy flux density at different angles of incidence

The Fresnel concentrator system is designed to capture incidence light reaching the Fresnel lens surface; however, due to system installation errors, tracking errors, and changes in the solar radiation angle, the Fresnel lens surface is not perfectly perpendicular to the sun's rays, causing solar energy loss and a decline in the light concentration efficiency. The influence of the incidence angle cannot be determined in an experiment, as shown in Fig. 13(a), and a simulation is used to analyze the influence of different incidence angles on the performance of the Fresnel concentrator system. In addition, as shown in Fig. 13(b), when the rays originate from the right-hand side, the focus of the reflected rays moves towards the left.

The energy density of the solar cell gradually decreases with the increase in the incidence angle, as shown in Fig. 14. When the tracking is precise, the diagram shows an even distribution of the energy density

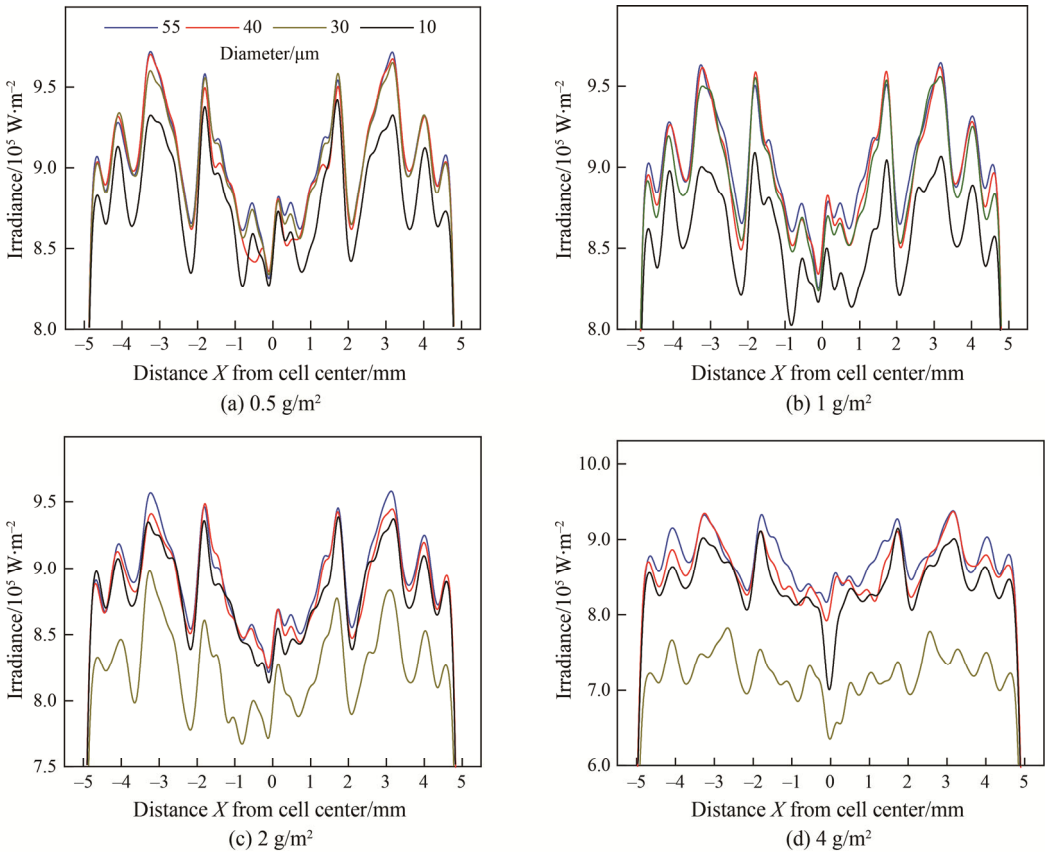

Fig. 11 Irradiance on the cell surface for dust particles with different diameters

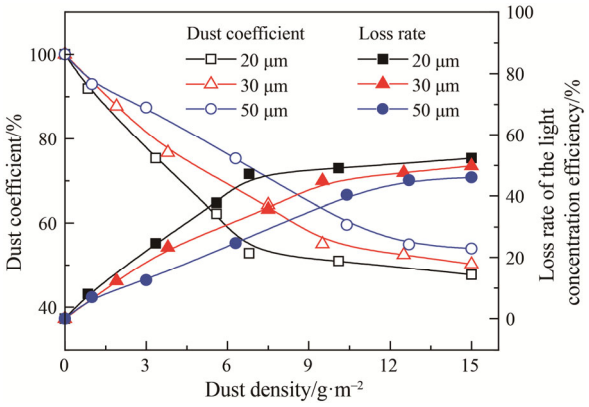

Fig. 12 Effect of the dust particle diameter on the dust coefficient and the loss rate of the light concentration efficiency

on the cell. As the incidence angle increases from 0° to 0.4°, some of the light is refracted or reflected, and the area of high energy density is shifted from the center to the edge at 5 mm from the center position. The area of high energy flux decreases from 1 cm^2 at an incidence angle of 0° to 0.15 cm^2 at an incidence angle of 0.5°, and the shape changes from a square to a strip. At an incidence angle of 0.9°, the energy density is relatively low.

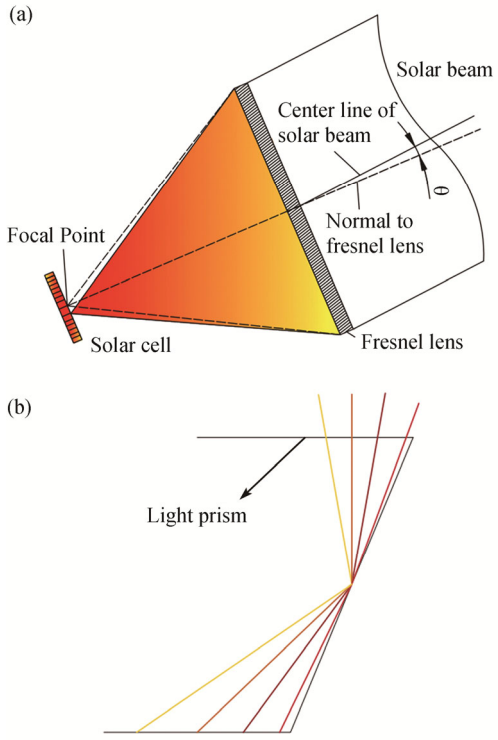

Fig. 13 Tracking error due to different incidence angles

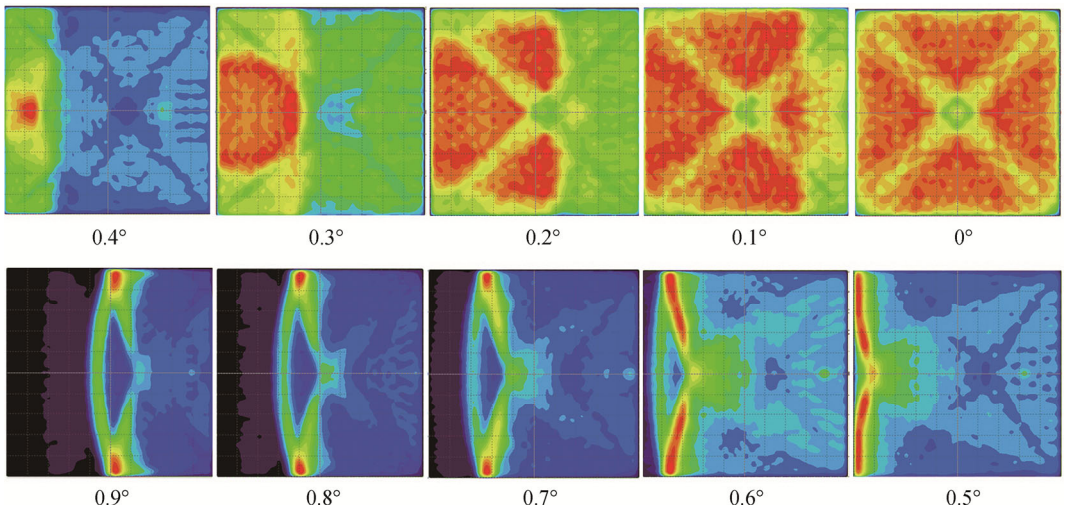

Fig. 14 Changes in the energy flux density with the increase in the incidence angle

Fig. 15 shows the light concentration efficiency at different angles of incidence for different dust densities. For the clean surface, the light concentration efficiency decreases by 28.53% for a 1° increase in the incidence angle. For the dust densities of 1.9 g/m^2 and 7.5 g/m^2, the decrease in the light concentration efficiency compared to the clean surface is 50.63% and 36.55%, respectively. At an incidence angle of 1°, the light concentration efficiency for the clean surface (0 g/m^2) and the dust densities of 1.9 g/m^2 and 7.5 g/m^2 is 58.99%, 51.76%, and 39.94%, respectively. Dust accumulation exacerbates the decrease in the light concentration efficiency as the incidence angle increases.

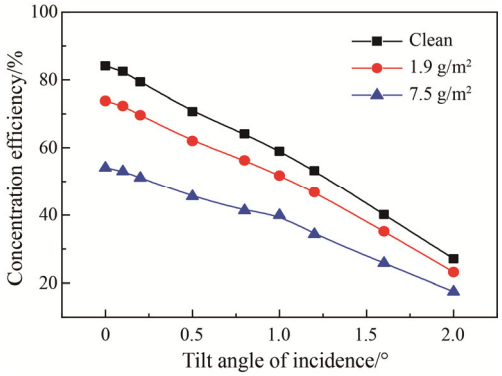

Fig. 15 Light concentration efficiency vs. the angle of incidence

4.4 Experimental analysis

Fig. 16 shows the solar spectral irradiance weighted by the standard AM 1.5G solar spectrum in the test area and the change in the lens sample transmittance at different wavelengths for the clean state. The transmittance of the sample was measured three times, and the results were averaged. The RMSE value of the three measurements was within 1%. The results were compared with the transmittance test of the PMMA lens with the same thickness [50]; the two curves show the same trend. However, the results obtained by Fu et al. [50] had a higher transmittance value and a faster response with the change in the transmittance than the experimental results. This result is attributed to the inherent properties of the materials.

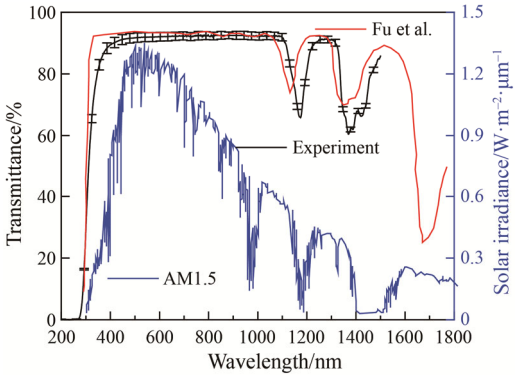

Fig. 16 Transmittance and solar irradiance at different wavelengths

Fig. 17 shows the lens transmittance at different dust densities. The transmittance was 91.71% for the clean surface and 40.39% at a dust density of 15.62 g/m^2. A linear relationship is observed, and for every 1 g/m^2 increase in the dust density, the transmittance decreases by 3.28%. In the study conducted by Al-Hasan [21], the transmittance decreased by 5.13% as the average dust density increased by 1 g/m^2. The difference in the transmittance is attributed to the difference in the dust material, which consisted of surface dust and sand particles, respectively.

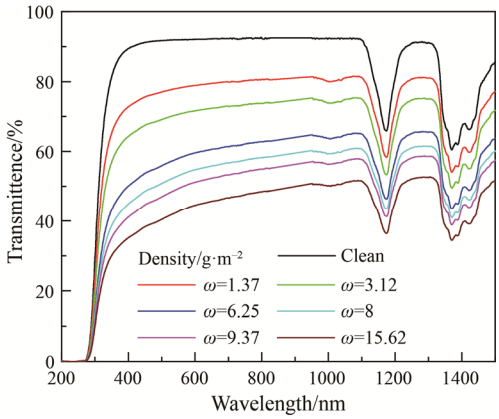

Fig. 17 Transmittance at different dust densities

A group of sieves combined with a screen vibrator was used to obtain the finest particles, and the smallest sieve sizes used were 50 μm and 60 μm. Fig. 18 shows that as the dust density increases, the light concentration efficiency exhibits a declining trend with a fast rate initially, followed by a slow rate. For the two cases, the light concentration efficiency decreases from 91.71% in the clean state to 40.39% and 41.16% at a dust density of 15 g/m^2. The light concentration efficiency decreases by 3.31% and 3.26% for an average increase in the dust density of 1 g/m^2, respectively. At the same dust density, the dust with a larger particle size has a smaller influence on the light concentration efficiency than the dust with smaller particle size; this result verifies the simulation results.

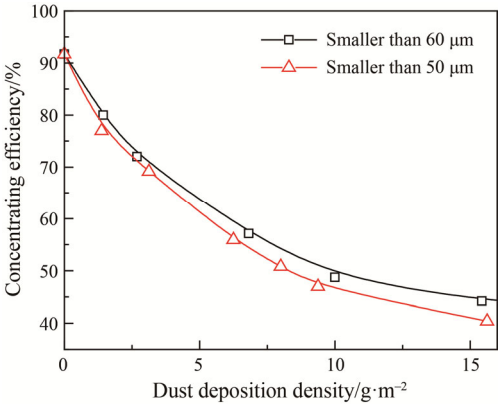

Fig. 18 Changes in the light concentration efficiency for different dust particle sizes

In Fig. 19, the simulation results for the dust particles with 50 μm diameter, and the experimental results of the light concentration efficiency for the dust particles smaller than or equal to 50 μm diameter are compared. Polynomial curve fitting was performed; the *R*-squared value was 0.934, and the maximum error was 5.74%. The error is attributed to the large range of dust particle sizes in the experiment. The good agreement of the simulation and experimental results indicates that the relationship between the light concentration efficiency and the dust density is linear for a given dust particle diameter.

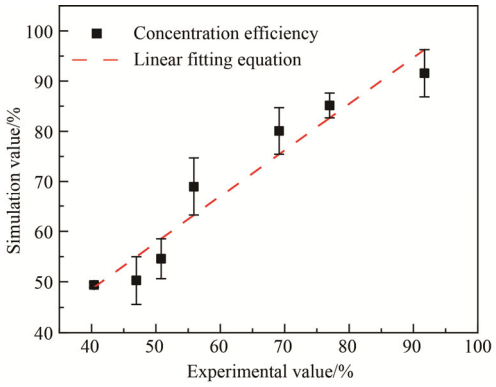

Fig. 19 Simulation and experimental results of the light concentration efficiency

5. Conclusions

A novel method was proposed to determine the optical light path at different dust densities on a Fresnel lens using the Tracepro software. The influences of the dust particle shape, diameter, and density on the light concentration efficiency of the HCPV/T system coupled with a Fresnel lens were investigated using the MCRT method. The simulation results and parameter settings were verified using experiments. The main conclusions are summarized as follows:

(1) A higher dust density and smaller particle size had greater influences on the light deflection angle. The triangular particles had stronger influences on the optical light path and the energy flux density than the circular and square particles.

(2) As the dust density increased, the energy flux density of the three dust particle shapes decreased in different degrees. As the dust density increased from the clean state to 15 g/m^2, a decrease in the light concentration efficiency of 67.1%, 64.4%, and 69.5% was observed for the circular, square, and triangular dust particles, respectively.

(3) The optical spot uniformity on the surface differed for the different particle shapes. In addition to the dust density, the influence of the light concentration efficiency also depended on the solar incidence angle.

(4) The largest changes in the light concentration efficiency were observed for the finest particles. For the experiments with particle sizes smaller than 50 μm and 60 μm, the light concentration efficiency decreased by 3.31% and 3.26%, respectively, for an average increase in the dust density of 1 g/m^2.

The results of this study can provide references for operators for cleaning Fresnel lenses to improve the thermoelectric output of the system.

Acknowledgments

This research was supported by the National Natural Science Foundation of China (No.51766012), the Natural Science Foundation of Inner Mongolia (No. 2019MS05025), the Inner Mongolia Science and Technology Major Project (No. 2019ZD014) and the Key Project of the ESI Discipline Development of Wuhan University of Technology (WUT Grant No. 2017001).

References

[1] Figgis B., Ennaoui A., Ahzi S., Rémond Y., Review of PV soiling particle mechanics in desert environments. Renewable and Sustainable Energy Reviews, 2017, 76: 872–881.

[2] Renno C., Thermal and electrical modelling of a CPV/T system varying its configuration. Journal of Thermal Science, 2019, 28: 123–132.

[3] Griffith DJ., Vhengani L., Maliage M., Measurements of mirror soiling at a candidate CSP site. Energy Procedia, 2014, 49: 1371–1378.

[4] Siddiqui R., Bajpai U., Correlation between thicknesses of dust collected on photovoltaic module and difference in efficiencies in composite climate. International Journal of Energy and Environmental Engineering, 2012, 3: 26–33.

[5] Jin Y., Fang J., Wei J., Qaisrani M.A., Wang X., Thermal performance evaluation of a cavity receiver based on particle's radiation properties during the day time. Renewable Energy, 2019, 143: 622–636.

[6] Kalogirou S.A., Agathokleous R., Panayiotou G., On-site PV characterization and the effect of soiling on their performance. Energy, 2013, 51: 439–446.

[7] Goswami D.Y., Vijayaraghavan S., Lu S., Tamm G., New and emerging developments in solar energy. Solar Energy, 2004, 76: 33–43.

[8] Abdolzadeh M., Nikkhah R., Experimental study of dust deposition settled over tilted PV modules fixed in different directions in the southeast of Iran. Environmental Science and Pollution Research, 2019, 26(30): 31478–31490.

[9] Jesus MAML de, Timò G., Agustín-Sáenz C., Braceras I., Cornelli M., Ferreira A de M., Anti-soiling coatings for solar cell cover glass: Climate and surface properties influence. Solar Energy Materials and Solar Cells, 2018, 185: 517–523.

[10] Kazem H.A., Chaichan M.T., The effect of dust accumulation and cleaning methods on PV panels' outcomes based on an experimental study of six locations in Northern Oman. Solar Energy, 2019, 187: 30–38.

[11] Maghami M.R., Hizam H., Gomes C., Radzi M.A., Rezadad M.I., Hajighorbani S., Power loss due to soiling on solar panel: A review. Renewable and Sustainable Energy Reviews, 2016, 59: 1307–1316.

[12] Sayyah A., Horenstein M.N., Mazumder M.K., Energy yield loss caused by dust deposition on photovoltaic panels. Solar Energy, 2014, 107: 576–604.

[13] Darwish Z.A., Kazem H.A., Sopian K., Al-Goul M.A., Alawadhi H., Effect of dust pollutant type on photovoltaic performance. Renewable and Sustainable Energy Reviews, 2015, 41: 735–744.

[14] Ferrada P., Olivares D., del Campo V., Marzo A., Araya F., Cabrera E., et al., Physicochemical characterization of soiling from photovoltaic facilities in arid locations in the Atacama Desert. Solar Energy, 2019, 187: 47–56.

[15] Wu Z., Yan S., Wang Z., Ming T., Zhao X., Ma R., et al., The effect of dust accumulation on the cleanliness factor of a parabolic trough solar concentrator. Renewable Energy, 2020, 152: 529–539.

[16] Salari A., Hakkaki-Fard A., A numerical study of dust deposition effects on photovoltaic modules and photovoltaic-thermal systems. Renewable Energy, 2019, 135: 437–449.

[17] Lu H., Zhang L.Z., Influences of dust deposition on ground-mounted solar photovoltaic arrays: A CFD simulation study. Renewable Energy, 2019, 135: 21–31.

[18] Hachicha A.A., Al-Sawafta I., Said Z., Impact of dust on the performance of solar photovoltaic (PV) systems under United Arab Emirates weather conditions. Renewable Energy, 2019, 141: 287–297.

[19] Boyle L., Flinchpaugh H., Hannigan M.P., Natural soiling of photovoltaic cover plates and the impact on transmission. Renewable Energy, 2015, 77: 166–173.

[20] Pan A., Lu H., Zhang L.Z., Experimental investigation of dust deposition reduction on solar cell covering glass by different self-cleaning coatings. Energy, 2019, 181: 645–653.

[21] Al-Hasan A.Y., A new correlation for direct beam solar radiation received by photovoltaic panel with sand dust accumulated on its surface. Solar Energy, 1998, 63: 323–333.

[22] Wang H., Meng X., Chen J., Effect of air quality and dust deposition on power generation performance of photovoltaic module on building roof. Building Services Engineering Research and Technology, 2020, 41: 73–85.

[23] Alnasser T.M.A., Mahdy A.M.J., Abass K.I., Chaichan M.T., Kazem H.A., Impact of dust ingredient on photovoltaic performance: An experimental study. Solar Energy, 2020, 195: 651–659.

[24] Kaldellis J.K., Kapsali M., Simulating the dust effect on the energy performance of photovoltaic generators based on experimental measurements. Energy, 2011, 36: 5154–5161.

[25] Chanchangi Y.N., Ghosh A., Sundaram S., Mallick T.K., An analytical indoor experimental study on the effect of soiling on PV, focusing on dust properties and PV surface material. Solar Energy, 2020, 203: 46–68.

[26] Beattie N.S., Moir R.S., Chacko C., Buffoni G., Roberts S.H., Pearsall N.M., Understanding the effects of sand and dust accumulation on photovoltaic modules. Renewable Energy, 2012, 48: 448–452.

[27] Dahlioui D., Laarabi B., Barhdadi A., Investigation of soiling impact on PV modules performance in semi-arid and hyper-arid climates in Morocco. Energy for Sustainable Development, 2019, 51: 32–39.

[28] Kazem H.A., Chaichan M.T., Experimental analysis of the effect of dust's physical properties on photovoltaic modules in Northern Oman. Solar Energy, 2016, 139: 68–80.

[29] Parrott B., Carrasco Zanini P., Shehri A., Kotsovos K., Gereige I., Automated, robotic dry-cleaning of solar panels in Thuwal, Saudi Arabia using a silicone rubber brush. Solar Energy, 2018, 171: 526–533.

[30] Tanesab J., Parlevliet D., Whale J., Urmee T., Seasonal effect of dust on the degradation of PV modules performance deployed in different climate areas. Renewable Energy, 2017, 111: 105–115.

[31] Hachicha A.A., Al-Sawafta I., Ben Hamadou D., Numerical and experimental investigations of dust effect on CSP performance under United Arab Emirates weather conditions. Renewable Energy. 2019, 143: 263–276.

[32] Mehmood U., Irshad H.M., Al-Sulaiman F.A., Bashir S., Yilbas B.S., Effect of accumulation of environmental dust and subsequent mud formation on textural, chemical, and optical properties of silicon wafers for photovoltaic cells. IEEE Journal of Photovoltaics, 2018, 8: 1274–1280.

[33] Buseck P.R., Pósfai M., Airborne minerals and related aerosol particles: Effects on climate and the environment. Proceedings of the National Academy of Sciences of the United States of America, 1999, 96: 3372–3379.

[34] Ghazi S., Sayigh A., Ip K., Dust effect on flat surfaces - A review paper. Renewable and Sustainable Energy Reviews, 2014, 33: 742–751.

[35] Mishra S.K., Agnihotri R., Yadav P.K., Singh S., Prasad M., Praveen P.S., et al., Morphology of atmospheric particles over semi-arid region (Jaipur, Rajasthan) of India: Implications for optical properties. Aerosol and Air Quality Research, 2015, 15: 974–984.

[36] El-Shobokshy M.S., Hussein F.M., Effect of dust with different physical properties on the performance of photovoltaic cells. Solar Energy, 1993, 51: 505–511.

[37] Heimsath A., Nitz P., The effect of soiling on the reflectance of solar reflector materials - Model for prediction of incidence angle dependent reflectance and attenuation due to dust deposition. Solar Energy Materials and Solar Cells, 2019, 195: 258–268.

[38] Renno C., Landi G., Petito F., Neitzert H.C., Influence of a degraded triple-junction solar cell on the CPV system performances. Energy Conversion and Management, 2018, 160: 326–340.

[39] Imtiaz Hussain M., Lee G.H., Experimental and numerical studies of a U-shaped solar energy collector to track the maximum CPV/T system output by varying the flow rate. Renewable Energy, 2015, 76: 735–742.

[40] Wu G., Yang Q., Zhang Y., Fang H., Feng C., Zheng H., Energy and optical analysis of photovoltaic thermal integrated with rotary linear curved Fresnel lens inside a Chinese solar greenhouse. Energy, 2020, 197: 117215.

[41] Li G., Design and development of a lens-walled compound parabolic concentrator-a review. Journal of Thermal Science, 2019, 28: 17–29.

[42] Yan S., Zhao S., Ma X., Ming T., Wu Z., Zhao X., et al., Thermoelectric and exergy output performance of a Fresnel-based HCPV/T at different dust densities. Renewable Energy, 2020, 159: 801–811.

[43] Katzan C.M., Edwards J.L., Lunar dust transport and potential interactions with power system components. NASA Contractor Report 4404, 1991.

[44] Liang H., Fan M., You S., Zheng W., Zhang H., Ye T., et al., A Monte Carlo method and finite volume method coupled optical simulation method for parabolic trough solar collectors. Applied Energy, 2017, 201: 60–68.

[45] Feng G., Li P., He Y., Wang Y., Wu H., Uncertainties evaluations in the ray-tracing algorithm based on Monte Carlo method. 7th International Symposium on Advanced Optical Manufacturing and Testing Technologies: Design, Manufacturing, and Testing of Micro- and Nano-Optical Devices and Systems, 2014, 9283: 92830Y.

[46] Ho W.H., Tsai J.T., Lin B.T., Chou J.H., Adaptive network-based fuzzy inference system for prediction of surface roughness in end milling process using hybrid Taguchi-genetic learning algorithm. Expert Systems with Applications, 2009, 36: 3216–3222.

[47] Jiang H., Lu L., Sun K., Experimental investigation of the impact of airborne dust deposition on the performance of solar photovoltaic (PV) modules. Atmospheric Environment, 2011, 45: 4299–4304.

[48] Meng Q., Wang Y., Zhang L., Irradiance characteristics and optimization design of a large-scale solar simulator. Solar Energy, 2011, 85: 1758–1767.

[49] Bohren C.F., Huffman D.R., Absorption and scattering of light by small particles. Arizona, United States of America, 1998.

[50] Fu L., Leutz R., Annen H.P., Evaluation and comparison of different designs and materials for Fresnel lens-based solar concentrators. Nonimaging Optics: Efficient Design for Illumination and Solar Concentration VIII, 2011, 8124: 81240E.